Available online at www.sciencedirect.com
ScienceDirect
Journal of Nuclear Materials 361 (2007) 174–183
journal of nuclear materials
www.elsevier.com/locate/jnucmat

Thermal and radiation-induced segregation in model Ni-base alloys

T.R. Allen [a,*], L. Tan [a], G.S. Was [b], E.A. Kenik [c]

[a] University of Wisconsin, Madison, WI, USA
[b] University of Michigan, Ann Arbor, MI, USA
[c] Oak Ridge National Laboratory, Oak Ridge, TN, USA

Abstract

Since Generation IV nuclear energy systems will operate at higher temperatures than current light water reactors, Ni-base alloys are receiving attention as candidate core materials. One aspect of the radiation response of Ni-base alloys to radiation that is not well understood is grain boundary segregation. In this work, three alloys, specifically Ni–18Cr, Ni–18Cr–9Fe, and Ni–18Cr–0.08P were given a series of thermal treatments and quenching to understand the development of thermal non-equilibrium segregation (TNES). Additionally, they were irradiated using 3.2 MeV protons at temperatures from 200 to 500 °C to doses up to 1 dpa. Grain boundary segregation was measured with Auger Electron Spectroscopy and Scanning Transmission Electron Microscopy with Energy Dispersive Spectroscopy. Chromium enrichment due to TNES could be caused by interactions between Ni and Cr or by interactions with impurity elements such as B, C, or N. Under irradiation, the addition of iron to Ni–18Cr reduced the grain boundary chromium depletion, while the addition of phosphorous increased the grain boundary chromium depletion.

PACS: 61.80−x; 61.80.Jh; 64.75+g

1. Introduction

Generation IV nuclear energy systems will operate at higher temperatures than current light water reactors, leading to an increased examination of Ni-base alloys for core material application. One aspect of the radiation response of Ni-base alloys to radiation that is not well understood is radiation-induced segregation at grain boundaries. Radiation-induced segregation is a non-equilibrium process that occurs at grain boundaries and other defect sinks such as dislocation loops and voids during irradiation of an alloy at high-temperature (30–50% of the melting temperature in K) [1]. In irradiated iron-base austenitic alloys, nickel enriches and chromium depletes at defect sinks. Iron either enriches or depletes depending on the bulk alloy composition. Studies have shown that the segregation to defect sinks such as dislocation loops and voids may play an important role in microstructural development [2–5].

* Corresponding author. Tel.: +1 608 265 4083; fax: +1 608 263 7451.
E-mail address: allen@engr.wisc.edu (T.R. Allen).

0022-3115/$ - see front matter © 2006 Elsevier B.V. All rights reserved.
doi:10.1016/j.jnucmat.2006.12.004

Thermal non-equilibrium segregation (TNES) at grain boundaries has also been observed to occur as a result of heat treatments [6]. Specifically, enrichment of grain boundary Cr has been observed to occur under certain heat treatment conditions (annealing temperature and cooling rates) in austenitic stainless steels [7–11]. As an example, studies by Cole et al. [8] on a series of Fe–Cr–Ni–Mo–P alloys indicated that TNES caused Cr, Mo, and P enrichment and Fe and Ni depletion. The studies varied both the starting temperature (from 1100 to 1300 °C) as well as the cooling method (furnace cool, air cool, water quench, and brine water quench) to show that grain boundary chromium enrichment caused by TNES was maximized when starting from lower annealing temperatures and using the slower cooling rates. For Fe-base austenitic alloys that exhibit Cr enrichment due to TNES, subsequent irradiation leads to chromium depletion due to RIS, but an intermediate 'W-shaped' profile is formed with Cr depletion to either side of the grain boundary and Cr enrichment on the boundary. At high dose, the 'W' profile is eliminated and chromium depletes at the boundary.

To gain an understanding of RIS and TNES in nickel-base alloys, Ni–18Cr, Ni–18Cr–9Fe, and Ni–18Cr–0.08P were studied. RIS and TNES were measured following irradiation and following heat treatment.

2. Experiments

Three alloys were studied, specifically Ni–18Cr, Ni–18Cr–9Fe, and Ni–18Cr–0.08P and were chosen to form alloy pairs to determine the effect of specific alloying additions. The alloy pairs are: a binary concentrated alloy (Ni–18Cr) and a ternary concentrated alloy (Ni–18Cr–9Fe) to investigate the effect of adding a concentrated third element; and a binary concentrated alloy (Ni–18Cr) and a binary concentrated alloy with a dilute impurity (Ni–18Cr–0.08P) to investigate the effect of adding a dilute third element. All three alloys have similar bulk chromium concentration. The General Electric Company supplied the alloys. Table 1 lists the compositions. Major alloying element compositions were determined by electron microprobe analysis. All three alloys form equilibrium fcc solid solutions at all temperatures of interest in this study.

Sample preparation prior to irradiation produced samples with a grain size in the range of 10–15 μm to ensure entire grains will be irradiated to a uniform dose when using a 3.2 MeV proton beam. Alloys were received in the form of 15–17 mm thick ingots. The ingots were cold-rolled to 12 mm thick then solution annealed at 1200 °C for 1 h. Portions of the solution annealed ingot were cold rolled to 3.5–5 mm thick and cut into Auger Electron Spectroscopy (AES) and scanning transmission electron microscopy with energy dispersive spectroscopy (STEM/EDS) sample bars. AES sample bars were approximately 2 mm wide, 2 mm thick and at least 25 mm long. STEM/EDS sample bars were approximately 4 mm wide, 2 mm thick and at least 25 mm long. After mechanical polishing, the samples were given a recrystallization anneal to obtain a grain size of 10–15 μm. To achieve this grain size, the samples were heated to 750 °C for 30 min.

Sample irradiations were performed using the General Ionex Tandetron accelerator at the Michigan Ion Beam Laboratory. Irradiations were conducted using 3.2 MeV protons at a dose rate of approximately 7×10^{-6} dpa/s (the experimental doses and dose rates reported throughout this paper are calculated using TRIM90 [12], resulting in a nearly uniform damage rate through the first 35 μm of the proton range (45 μm)). With a grain size of 10–15 μm, multiple grain depths are irradiated. Samples were irradiated at temperatures from 200 to 500 °C to 0.5 dpa and at 400 °C to 1 dpa.

To determine the effect of TNES on grain boundary composition, four separate heat treatment and

Table 1
Summary of bulk alloy compositions in at.% (second line gives normalized compositions for Fe + Cr + Ni + P = 100%)

Alloy	Cr	Ni	Fe	Mn	Mo	Si	C	P	S
Ni–18Cr	18.24	81.74	–	–	0.002	–	0.005	0.006	0.004
	18.24	81.75	–					0.006	
Ni–18Cr–9Fe	18.26	72.36	9.32	0.010	0.002	0.027	0.014	0.007	0.004
	18.26	72.39	9.33					0.007	
Ni–18Cr–0.08P	18.33	81.56	0.004	–	0.06	0.012	0.004	0.08	–
	18.33	81.58	0.004					0.08	

cooling regimes were carried out. These treatments all used the material cold rolled to 3.5–5 mm thickness as the starting point and then performed one of the following:

- Anneal at 1100 °C for 15 min followed by water quench (designated 1100_W).
- Anneal at 1100 °C for 15 min followed by furnace cool (designated 1100_F).
- Anneal at 750 °C for 15 min followed by water quench (designated 750_W_15).
- Anneal at 750 °C for 30 min followed by water quench (designated 750_W_30).

To promote intergranular fracture of AES bars, a small notch was cut on one surface and then the sample was hydrogen charged using 0.1 N sulfuric acid with the addition of sodium arsenite as a poison for recombination of hydrogen. Sample bars were fractured in situ at a pressure of 1×10^{-9} Torr by bending with a special fracture stage attached to the vacuum chamber. Once the fracture was achieved, secondary electron images (SEIs) were used to capture major fracture features, specifically intergranular (IG) and ductile (*D*) areas.

A PHI 660 scanning Auger electron spectrometer was used to analyze microchemistry at interfaces of RIS samples. A PHI 670 scanning Auger electron spectroscope was used to analyze microchemistry at interfaces of TNES samples. Results of chemical composition are reported as atomic concentration calculated following Davis et al. [13]. Sensitivity factors of iron, chromium, and nickel have been obtained by comparing calculated concentration for the ductile areas of as-received sample to the composition of the material measured using electron microprobe analysis. Because of the low *P* concentrations in the bulk material, this technique could not be used for determining the sensitivity factor of phosphorous so the system default sensitivity factor was used.

The STEM/EDS was performed at Oak Ridge National Laboratory using a Phillips EM400T/FEG equipped with an EDAX 9100/70 EDS system. An accelerating voltage of 100 kV was used. A double-tilt, liquid-nitrogen-cooled specimen holder was used to minimize contamination of the sample under the focused beam [14]. STEM/EDS measurements were performed at the grain boundary and at increments of 2.5 nm away from the boundary to give compositional profiles. The incident probe diameter was 2 nm (full width, tenth maximum). The sample was tilted towards the X-ray detector and each grain boundary analyzed was aligned such that the boundary was 'edge-on' (parallel to the electron beam). This placement minimizes the apparent, geometric broadening of the RIS profile, ensuring that the measured X-ray intensity at the grain boundary was the best estimate of the grain boundary composition.

3. Results

The TNES measurements (only AES measurements were taken) are summarized in Table 2. The RIS measurements are summarized in Table 3

Table 2
Summary of AES TNES measurements (uncertainty given by the standard deviation of the mean $\sigma/\sqrt{N}$) [15]

Alloy	Annealing temperature (°C)	Quench method	Fe (at.%)	Cr (at.%)	Ni (at.%)	Measurements
AES						
Ni–18Cr	1100	Furnace	–	19.1 ± 0.0	80.9 ± 0.0	12
Ni–18Cr	1100	Water	–	16.7 ± 0.3	83.3 ± 0.3	16
Ni–18Cr	750 (15 min)	Water	–	17.3 ± 0.1	82.7 ± 0.1	15
Ni–18Cr	750 (30 min)	Water	–	17.1 ± 0.2	82.9 ± 0.2	12
Ni–18Cr–9Fe	1100	Furnace	8.3 ± 0.2	20.0 ± 0.7	71.7 ± 0.6	13
Ni–18Cr–9Fe	1100	Water	8.8 ± 0.2	19.5 ± 0.4	71.7 ± 0.4	19
Ni–18Cr–9Fe	750 (15 min)	Water	11.3 ± 0.6	17.9 ± 0.6	70.8 ± 1.0	16
Ni–18Cr–9Fe	750 (30 min)	Water	9.4 ± 0.3	18.0 ± 0.4	72.6 ± 0.5	12
P (at.%)						
Ni–18Cr–P	1100	Furnace	5.6 ± 0.4	16.4 ± 0.5	77.9 ± 0.6	10
Ni–18Cr–P	1100	Water	6.1 ± 0.4	16.7 ± 0.6	77.1 ± 0.6	16
Ni–18Cr–P	750 (15 min)	Water	7.6 ± 0.3	14.9 ± 0.3	77.4 ± 0.3	13
Ni–18Cr–P	750 (30 min)	Water	9.1 ± 0.4	14.0 ± 0.2	76.9 ± 0.3	10

All TNES measurements came from a single sample for each treatment.

Table 3
Summary of AES RIS measurements (uncertainty given by the standard deviation of the mean $\sigma/\sqrt{N}$) [15]

Alloy	Temperature (°C)	Dose (dpa)	Fe (at.%)	Cr (at.%)	Ni (at.%)	Measurements	Samples
AES							
Ni–18Cr	200	0.5	–	14.6 ± 0.2	85.4 ± 0.2	28	2
Ni–18Cr	300	0.5	–	11.5 ± 0.2	88.5 ± 0.2	33	2
Ni–18Cr	400	0.5	–	10.1 ± 0.2	89.9 ± 0.2	62	5
Ni–18Cr	500	0.5	–	12.9 ± 0.5	87.1 ± 0.5	23	2
Ni–18Cr–9Fe	200	0.5	6.7 ± 0.5	15.7 ± 0.2	77.6 ± 0.5	16	1
Ni–18Cr–9Fe	300	0.5	5.4 ± 0.5	13.8 ± 0.3	80.8 ± 0.6	14	1
Ni–18Cr–9Fe	400	0.5	5.8 ± 0.3	13.5 ± 0.2	80.7 ± 0.5	27	2
Ni–18Cr–9Fe	500	0.5	6.5 ± 0.3	15.7 ± 0.2	77.8 ± 0.5	30	2
Ni–18Cr	–	0.0	–	17.1 ± 0.2	82.9 ± 0.2	12	1
Ni–18Cr	400	0.1	–	13.4 ± 0.3	86.6 ± 0.3	33	2
Ni–18Cr	400	0.3	–	11.8 ± 0.2	88.2 ± 0.2	32	2
Ni–18Cr	400	1.0	–	10.6 ± 0.3	89.4 ± 0.3	36	2
Ni–18Cr–9Fe	–	0.0	9.4 ± 0.3	18.0 ± 0.4	72.6 ± 0.5	12	2
Ni–18Cr–9Fe	400	0.1	5.2 ± 0.2	13.9 ± 0.2	80.9 ± 0.3	23	2
Ni–18Cr–9Fe	400	0.3	4.9 ± 0.3	13.9 ± 0.4	81.1 ± 0.4	23	2
Ni–18Cr–9Fe	400	1.0	5.5 ± 0.3	13.8 ± 0.3	80.7 ± 0.6	27	2
P (at.%)							
Ni–18Cr–P	–	0.0	9.0 ± 0.4	14.0 ± 0.2	76.9 ± 0.3	10	1
Ni–18Cr–P	400	0.5	12.2 ± 0.3	8.7 ± 0.1	79.2 ± 0.4	24	2

(AES measurements) and Table 4 (STEM/EDS measurements). The trends in RIS are similar with each measurement technique. The depth resolution of the AES is better and gives a closer estimate of the actual grain boundary composition. The focus of the analysis will be on the AES measurements.

Fig. 1 shows the change in grain boundary chromium and nickel concentration for Ni–18Cr for the four different heat treatments used to induce TNES. All of the water quenched specimens exhibited chromium depletion and nickel enrichment. The sample cooled using furnace cooling exhibited chromium enrichment and nickel depletion.

Fig. 2 shows the change in grain boundary chromium and nickel concentration for Ni–18Cr–0.08P for the four different heat treatments used to induce TNES. Phosphorous enrichment, chromium depletion, and nickel depletion is seen for every treatment. The enrichment of phosphorous is greater when starting at a lower annealing temperature. The magnitude of phosphorous enrichment and chromium enrichment changes with treatment, but the nickel depletion is roughly constant.

Fig. 3 shows the change in grain boundary chromium and nickel concentration for Ni–18Cr–9Fe for the four different heat treatments used to induce

Table 4
Summary of STEM/EDS RIS measurements (uncertainty given by the standard deviation of the mean $\sigma/\sqrt{N}$) [15]

Alloy	Temperature (°C)	Dose (dpa)	Iron (at.%)	Chromium (at.%)	Nickel (at.%)	Measurements	Samples
STEM/EDS							
Ni–18Cr	400	0.0	–	18.8 ± 0.2	81.2 ± 0.2	15	1
Ni–18Cr	400	0.1	–	15.7 ± 0.2	84.3 ± 0.2	22	2
Ni–18Cr	400	0.3	–	14.3 ± 0.3	85.7 ± 0.3	34	2
Ni–18Cr	400	0.5	–	13.0 ± 0.3	87.0 ± 0.3	33	2
Ni–18Cr	400	1.0	–	13.6 ± 0.3	86.4 ± 0.3	15	1
Ni–18Cr–9Fe	400	0.0	9.2 ± 0.1	17.9 ± 0.2	72.8 ± 0.2	17	1
Ni–18Cr–9Fe	400	0.1	6.6 ± 0.1	16.0 ± 0.2	77.4 ± 0.3	22	2
Ni–18Cr–9Fe	400	0.3	5.8 ± 0.1	15.4 ± 0.2	78.7 ± 0.2	18	1
Ni–18Cr–9Fe	400	0.5	5.4 ± 0.1	14.4 ± 0.2	80.2 ± 0.3	45	2
Ni–18Cr–9Fe	400	1.0	5.8 ± 0.2	15.3 ± 0.2	78.7 ± 0.3	20	1

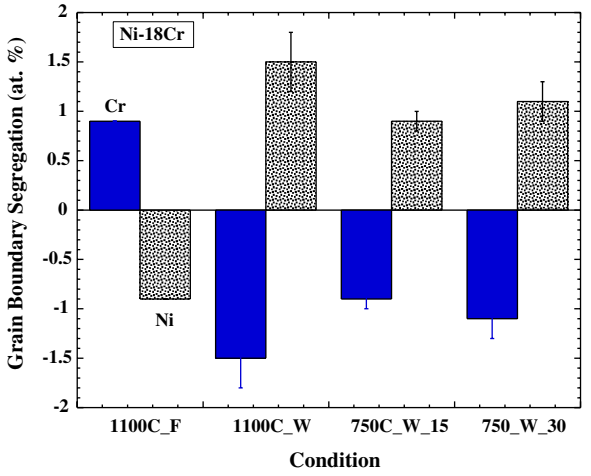

Fig. 1. Change in grain boundary chromium and nickel concentration for Ni–18Cr using four different combinations of annealing temperature and cooling method.

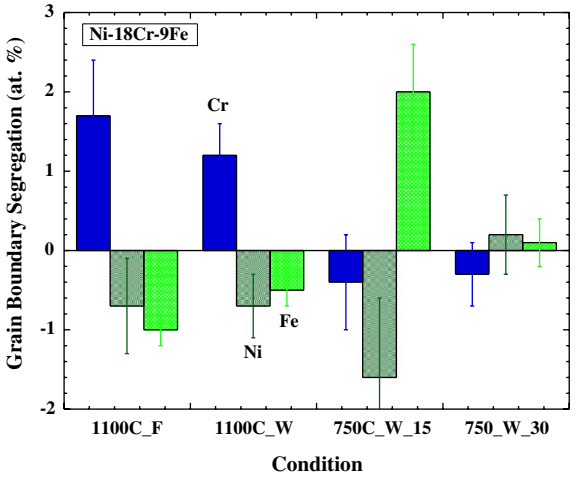

Fig. 3. Change in grain boundary chromium and nickel concentration for Ni–18Cr–9Fe using four different combinations of annealing temperature and cooling method.

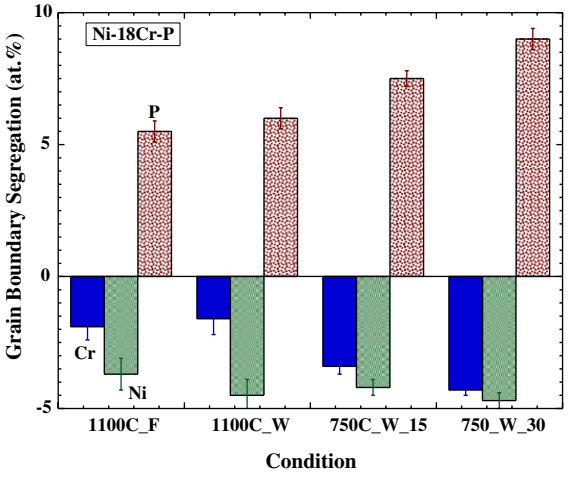

Fig. 2. Change in grain boundary chromium and nickel concentration for Ni–18Cr–0.08P using four different combinations of annealing temperature and cooling method.

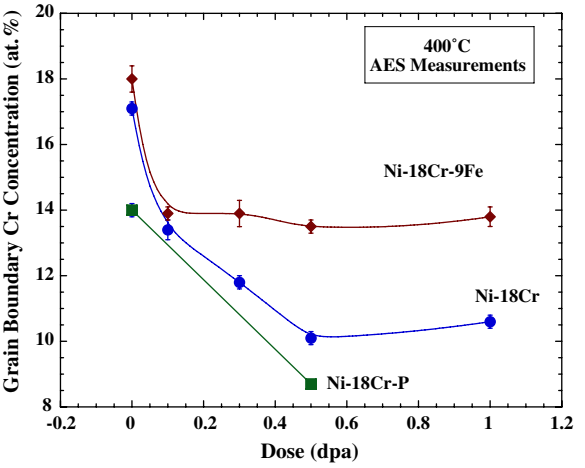

Fig. 4. Grain boundary chromium concentration for Ni–18Cr, Ni–18Cr–9Fe, and Ni–18Cr–0.08P irradiated at 400 °C.

TNES. Chromium enrichment occurs for both treatments that use an 1100 °C anneal, while chromium depletion occurs for all treatments that use a 750 °C anneal. For the 1100 °C anneals, slightly more Cr enrichment occurs under furnace cooling.

Figs. 4 and 5 show the grain boundary chromium and nickel concentration, measured using AES, as a function of dose for samples irradiated at 400 °C. As noted in the experiment section, these samples were cold-rolled and annealed at 750 °C prior to irradiation. Although not plotted, the STEM/EDS measurements follow a similar trend. Due to greater averaging across the profile when using the STEM/EDS technique, the measured STEM/EDS value always indicates less enrichment or depletion than the AES measurement. The addition of iron to Ni–18Cr reduces the grain boundary chromium depletion and reduces the grain boundary nickel enrichment. The addition of phosphorous increases the chromium depletion and reduces the nickel enrichment. Fig. 6 shows the grain boundary chromium concentration, as measured using AES, for Ni–18Cr and Ni–18Cr–9Fe as a function of temperature for samples irradiated to 0.5 dpa. For both alloys, the segregation reaches a maximum at a temperature near 400 °C, with the Ni–18Cr sample

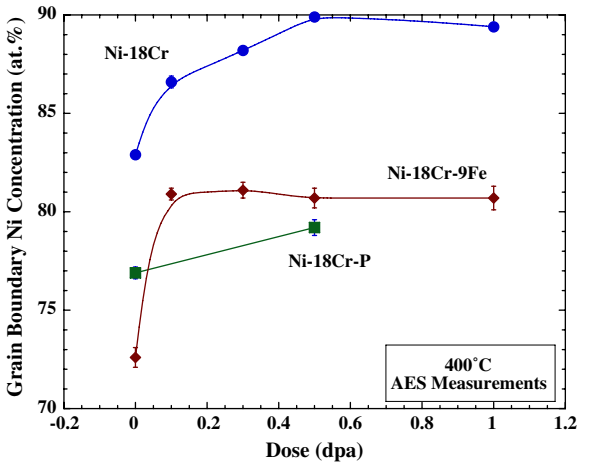

Fig. 5. Grain boundary nickel concentration for Ni–18Cr, Ni–18Cr–9Fe, and Ni–18Cr–0.08P irradiated at 400 °C.

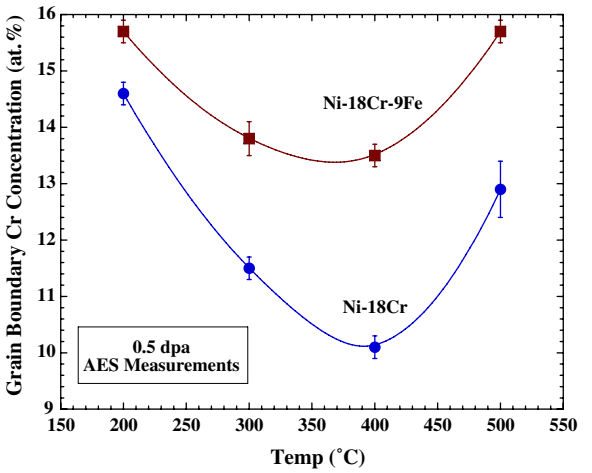

Fig. 6. Grain boundary chromium concentration for Ni–18Cr and Ni–18Cr–9Fe irradiated to 0.5 dpa from 200 to 500 °C.

possibly having maximum chromium depletion at slightly higher temperature. Although not shown, the grain boundary segregation profiles on the Ni–18Cr and Ni–18Cr–9Fe alloys, measured using STEM/EDS, do not show any evidence of a 'W-shaped' segregation profile at any dose.

4. Discussion

4.1. Thermal non-equilibrium segregation

In Ni–18Cr, when annealed and then water quenched, Cr depletes and Ni enriches at grain boundaries. The segregation is greater at higher temperature. On the other hand, when furnace cooling is used, establishing conditions where TNES is expected, Cr enriches, consistent with Fe-base austenitic alloys. If the Cr depletion during annealing were caused by Gibbsian segregation, the segregation energy calculated from the measured enrichment would be on the order of 0.005–0.01 eV, a very small energy. For conditions where TNES occurs, Cr can enrich in a simple binary alloy. Therefore, Cr enrichment via TNES may be energetically favorable based on coupling to the vacancy flux or it is driven by an interaction with some element at the grain boundary.

Simonen et al. [15], modeled TNES and RIS of chromium in an Fe–Cr–Ni system. Two driving mechanisms for Cr diffusion were assumed, exchange of the Cr atoms with the vacancies, driving Cr away from the boundary with a characteristic Cr–vacancy migration energy and Cr–vacancy complexes dragging Cr to the boundary with a characteristic binding energy. The simple model used did not attempt to describe interactions between Cr and other atoms in the system. He found that no reasonable combination of choices for the Cr–vacancy migration energy and Cr–vacancy binding energy were able to explain the observed TNES of Cr or the 'W' shaped profiles formed under irradiation. His conclusion was that interactions with other elements (beyond Cr–vaccany complexes) must be involved. Kenik et al., studied TNES in commercial purity 304 and 316 stainless steels and found enrichment of the interstitial impurities B, C, and N at boundaries, with a pronounced affinity between Mo and N [16]. Thus, interactions with a minor element may contribute to TNES. One other possibility, similar to the effect that will be described below for RIS, is that Cr is attracted to Ni. Under annealing, Ni is enriched at the boundary in Ni–18Cr, and may provide an attractive force to Cr atoms under the large flux of vacancies to the grain boundary under TNES conditions.

As shown in Fig. 2, for the Ni–18Cr–0.08P alloy, Cr does not enrich under any thermal treatment. The depletion of nickel is relatively constant, with P enrichment and Cr depletion changing with heat treatment. Chromium depletion in Ni–18Cr–0.08P is consistent with the water-cooled samples in Ni–18Cr, but chromium depletion following furnace cooling in Ni–18Cr–0.08P is the opposite to that seen in Ni–18Cr. Cr does not appear to be preferentially attracted to phosphorous, indicating Cr–P interactions are not a driver for the TNES enrich-

ment of Cr (or as possible a contributor to the formation of 'W' shaped Cr segregation profiles under radiation).

For the Ni–18Cr–9Fe alloy, the results are ambiguous. The Cr enrichment with water quench and furnace cooling at 1100 °C, with greater enrichment for furnace cooling, is consistent with work by Cole on Fe–16Cr–13Ni alloys. The Cr depletion for samples annealed at 750 °C and then water quenched is consistent with the Ni–18Cr alloy.

Studies of TNES and subsequent RIS in Fe-base austenitic alloys exist in the literature [7–11]. These studies cover the 304, 316, and 321 alloy systems. According to the study by Cole et al., [8] the presence of Mo and P are not needed for TNES to occur. They also found that although the P grain boundary concentration is not significantly altered during irradiation, P does appear to reduce the extent of grain boundary Cr depletion. Was et al., [9] showed that, at grain boundaries in 304 and 316 stainless steel, the TNES-driven enrichment of Cr and Mo as well as Cr and Mo depletion under irradiation followed similar trends with both elements. With increasing radiation dose, the Cr went from enriched at the boundary, through the formation of a 'W' shaped profile, to depleted at the grain boundary. The trends were similar for both proton and neutron irradiated samples.

Table 5 summarizes the reported trends in segregation for various elements. The segregation trends fall into categories.

- Elements that deplete via TNES and remain depleted following RIS (Fe).
- Elements that enrich via TNES and remain enriched following RIS (P, Ti).
- Elements that enrich via TNES but deplete following RIS (Cr, Mo).
- Elements that deplete via TNES but enrich following RIS (Si, Ni).

Elements that are always depleted, like Fe, are not likely to cause 'W-shaped' RIS profiles as they are already depleted at the boundary. Elements that enrich via TNES and remain enriched following RIS like Ti and P are potential factors in causing the 'W' RIS profile of Cr. For example, an attractive force between Cr and P would conceivably retain Cr at the boundary even as Cr depletes off-boundary due to RIS. Despite this theoretical possibility, Ti is not in many alloys that show the 'W' profile and this study and the Cole study indicate Cr–P interactions are not the likely cause. Elements (other than Cr) that enrich via TNES but deplete following RIS, like Mo, are not likely causes since they are not remaining at the boundary to pin Cr. Finally, elements that deplete via TNES but enrich following RIS, like Si and Ni, might cause the 'W' profile by temporarily limiting vacancy flux of Cr away from boundary if they enrich fast enough. For these elements, the interaction force is not strong enough to prevent RIS, but changes the segregation path taken during RIS. Since the Cole study showed 'W' profiles without the presence of Si, Si is not a determining cause.

The data from this study, as well as the available literature, leave only two possibilities as potential causes for the 'W' shaped Cr depletions. The first is attractive ordering forces between Ni and Cr. The second is interactions with very small concentrations of interstitial impurity elements such as C, B and N. For Ni–Cr interactions, the tendency to short range order alters but does not change the final segregation, which is primarily driven by exchange of individual atoms with the point defect flux.

Table 5
Trends in segregation due to TNES and RIS in Fe-base austenitic alloys

Element	TNES	RIS	Link to TNES and 'W-shaped' RIS profile of Cr
P	E	E	Not supported by this study or by Cole study
Ti	E	E	Not in 304/316 so not necessary
Mo	E	D	Depletes at similar rate as Cr. Not supported by Cole study
Cr	E	D	–
Si	D	E	Not in Cole Fe–16Cr–13Ni + alloys so not necessary
Ni	D (small depletion or no segregation)	E	Interaction with Cr?
Fe	D	D	Not enriched at grain boundaries

E = enriched, D = depleted.

4.2. Radiation-induced segregation

The trends in RIS behavior as a function of alloy composition for Ni–18Cr and Ni–18Cr–9Fe are consistent with a vacancy-driven inverse Kirkendall mechanism, similar to that seen in austenitic Fe-base alloys [17]. The fast diffusing chromium (fast diffusing via interactions with the vacancy flux) depletes at the boundary while the slow moving nickel is enriched. Comparing Ni–18Cr to Ni–18Cr–9Fe, replacing 9 at.% of the slow diffusing Ni with faster diffusing Fe moves the Cr and Ni diffusivity closer to the alloy average, reducing the driving force for radiation-induced segregation. Thus, less chromium depletion and nickel enrichment is seen in Ni–18Cr–9Fe. The overall vacancy diffusivity is faster in Ni–18Cr–9Fe than in Ni–18Cr [18,19], driving the segregation to steady-state faster in Ni–18Cr–9Fe (see Fig. 4).

If segregation is measured in two alloys with different migration energies, the alloy with the smaller migration energy will have its maximum segregation at a lower temperature than the other alloy. Table 6 lists the self-diffusion energy for Cr in both Ni–18Cr and Ni–18Cr–9Fe. The self-diffusion energy for Cr is larger in Ni–18Cr. Assuming the corresponding Cr–vacancy migration energy is also larger ($E_{sd} = E_{formation} + E_{migration}$), then the maximum chromium depletion in Ni–18Cr, with a higher Cr–vacancy migration energy, should occur at a higher temperature than in Ni–18Cr–9Fe. This trend appears to be supported by the data in Fig. 6.

Strong P enrichment, even before irradiation, dominates grain boundary compositional changes in Ni–18Cr–0.08P. Nickel enrichment is retarded in Ni–18Cr–0.08P as compared to Ni–18Cr. Additionally, more chromium is displaced from the boundary with the phosphorous present. The change in chromium concentration is about 4 at.% in both Ni–18Cr and Ni–18Cr–0.08P so the kinetics of chromium depletion are similar in the two alloys. The main difference is that some nickel enrichment is replaced with phosphorous enrichment.

Table 6
Measured self-diffusion energies for Fe–20Cr–24Ni, Ni–18Cr, Ni–18Cr–9Fe

Alloy	Self-diffusion energy E_{sd}^{Cr} (eV)	Approximate temperature of minimum measured Cr (°C) concentration
Ni–18Cr	3.05 [16]	400
Ni–18Cr–9Fe	2.97 [17]	350

Even though the general trends (Cr depletion and Ni enrichment) of the RIS in the Ni–18Cr and Ni–Cr–Fe alloys are consistent with a vacancy-driven inverse Kirkendall mechanism, the magnitude of the segregation is not well predicted when using high-temperature vacancy diffusion data in an inverse Kirkendall model. Evidence suggests that attractive ordering forces between Ni and Cr alter the segregation predicted from high-temperature vacancy diffusion information. The details are given in ref [20] with an example given in Fig. 7. Fig. 7 plots the calculated and measured rate of exchange (dCr/dNi) of Cr and Ni at the grain boundary for Ni–18Cr–9Fe. dCr/dNi is calculated by plotting the Cr versus Ni concentration from both model predictions and AES data, fitting the Cr versus Ni plot with a second order polynomial, and then taking the derivative of the polynomial. Model calculations were performed using the Perks model [21] and assume that only the vacancy flux contributes to the grain boundary segregation (no differences in interstitial jump rates). From the model predictions in Fig. 7, as dose increases, Cr is replaced by Ni at the grain boundary at a slower rate. The dashed line at dCr/dNi = 0.5 indicates the point where half the Ni atoms arriving at the boundary are filling positions previously occupied by Cr atoms (the other positions being previously occupied by Fe atoms). Above the line, the majority of atoms leaving the boundary are Cr. At low dose, the model predicts that Cr leaves the boundary at a high rate. At higher doses, when the Cr at the boundary is sufficiently depleted, the model predicts that Cr is no longer dominant in exchanging with Ni, primarily because the predicted Cr concentration is significantly depleted at the boundary at high dose. dCr/dNi, calculated from *model predictions*, never reaches 0.5.

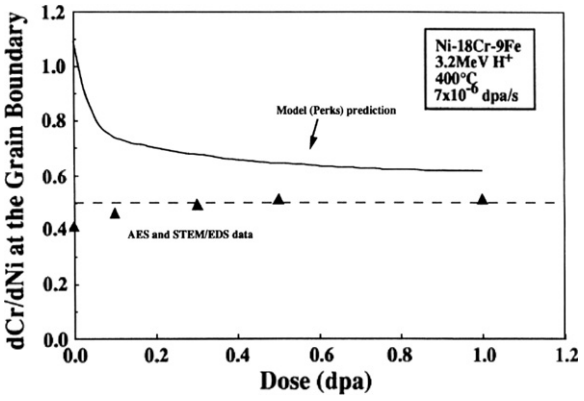

Fig. 7. Predicted and measured exchange rates (dCr/dNi) for Ni–18Cr–9Fe irradiated at 400 °C.

In the Ni–18Cr–9Fe alloy, dCr/dNi calculated from AES and STEM data varies in the opposite direction of that calculated from model predictions. The RIS data indicates that early in the irradiation, Cr is replaced by Ni at a much smaller rate than expected from calculation (indicating that Fe is replaced by Ni at a much higher rate than expected). At later stages in the irradiation, Cr and Fe are replaced with Ni at nearly equal rates. The measurements indicate that Fe diffuses at about the same rate as Cr in the Ni–18Cr–9Fe alloy, contrary to high-temperature diffusion measurements [19] that show Cr to be the faster diffuser. A possible explanation for the anomalous segregation behavior in the Ni–18Cr–9Fe alloy is strong attractive short range ordering forces between Cr and Ni. Many experiments have shown ordering to occur in Fe–Cr–Ni alloys, with ordering being more pronounced in Ni-base alloys [22–25]. The ordering forces used in RIS modeling of austenitic Fe-base alloys by Nastar [26] were −0.04 eV for Ni–Cr pairs, −0.03 eV for Ni–Fe pairs, and 0 eV for Fe–Cr pairs. The dominant ordering is characterized by the formation of Ni–Cr pairs. The tendency to form Ni–Cr pairs would slow down the Cr segregation relative to Fe at low dose.

5. Conclusions

Thermal non-equilibrium and radiation-induced segregation were studied in three alloys, Ni–18Cr, Ni–18Cr–0.08P, and Ni–18Cr–9Fe. Thermal treatments to cause TNES involved annealing at 750 and 1100 °C followed by either furnace cooling or water quenching. Radiations were conducted using high-energy protons at temperatures ranging from 200 to 500 °C and doses to 1.0 dpa.

Like TNES seen in Fe-base austenitic alloys, Cr enriches at grain boundaries when allowed to furnace cool following anneal. Examination of the TNES driven segregation in these Ni-base alloys, along with the TNES driven chromium enrichment reported in the literature for Fe-base austenitic alloys indicates that the 'W' profile seen in irradiated samples is not likely due to P at the grain boundary, but is more likely due to minor light elements (B, C, N) or attractive ordering forces between Ni and Cr.

General trends in radiation-induced segregation in these alloys were similar to that seen in austenitic stainless steels, with Ni enrichment and Cr depletion. The magnitude of the segregation, as compared to that predicted from high-temperature diffusion data, indicates that attractive forces between Ni and Cr may retard segregation.

Acknowledgements

Research sponsored by the Department of Energy, Office of Nuclear Energy, Science, and Technology under NERI Project 02–0110. Research at the Oak Ridge National Laboratory SHaRE User Facility was sponsored by the Division of Materials Sciences and Engineering, US Department of Energy under Contract DE-AC05-00OR22725 with UT-Battelle, LLC.

References

[1] P.R. Okamoto, L.E. Rehn, J. Nucl. Mater. 83 (1979).
[2] T.R. Allen, J.I. Cole, J. Gan, G.S. Was, R. Dropek, E.A. Kenik, J. Nucl. Mater. 342 (2005) 90.
[3] A. Si-Ahmed, W.G. Wolfer, in: H.R. Brager, J.S. Perrin (Eds.), Effects of Radiation on Materials: Eleventh Conference, ASTM STP 782, American Society for Testing and Materials, 1982, p. 1008.
[4] W.G. Wolfer, L.K. Mansur, J. Nucl. Mater. 91 (1980) 265.
[5] J.J. Sniegowski, W.G. Wolfer, in: Proc. of Topical Conference on Ferritic Alloys for Use in Nuclear Energy Technologies, Snowbird, Utah, 19–23 June, 1983.
[6] R.G. Faulkner, Int. Mater. Rev. 41 (5) (1996) 198.
[7] J.T. Busby, G.S. Was, S.M. Bruemmer, D.J. Edwards, E.A. Kenik, Mat. Res. Soc. Symp. Proc. Mater. Research Soc. 540 (1999) 451.
[8] J.I. Cole, T.R. Allen, G.S. Was, R.B. Dropek, E.A. Kenik, in: M.L. Grossbeck (Ed.), Effects of Radiation on Materials, ASTM STP 1447, ASTM International, West Conshohocken, PA, 2003, p. 540.
[9] G.S. Was, J.T. Busby, T. Allen, E.A. Kenik, A. Jenssen, S.M. Bruemmer, J. Gan, A.D. Edwards, P.M. Scott, P.L. Andresen, J. Nucl. Mater. 300 (2002) 198.
[10] P. Spellward, J. Walmsley, R. Scowen, N. Partridge, J. Stump, R. Corcoran, R. Gilmour, V. Callen, in: Proceedings of the Eighth International Symposium on Environmental Degradation of Materials in Nuclear Power Systems-Water Reactors, American Nuclear Society, p. 734.
[11] J.F. Williams, T.R. Mager, P. Spellward, M. Koyama, I. Suzuki, J. Walmsley, H. Mimaki, in: Proceedings of the Eighth International Symposium on Environmental Degradation of Materials in Nuclear Power Systems-Water Reactors, American Nuclear Society, p. 725.
[12] J.F. Ziegler, J.P. Biersack, TRIM 90 Program, IBM Corp. Yorktown, NY.
[13] L.E. Davis, N.C. MacDonald, P.W. Palmberg, G.E. Riach, R.E. Weber, Handbook of Auger Electron Spectroscopy, Physical Electronics Industries, Eden Prairie, MN, 1976.
[14] E.A. Kenik, Scripta Metall. 21 (1987) 811.
[15] E.P. Simonen, S.M. Bruemmer, in: Proceedings of the Eighth International Symposium on Environmental Degradation of Materials in Nuclear Power Systems – Water Reactors, Amelia Island, Florida, August 1997, American Nuclear Society, LaGrange Park, IL, 1997, p. 751.

[16] E.A. Kenik, J.T. Busby, M.K. Miller, A.M. Thuvander, G. Was, in: Proceedings of the MRS Fall Meeting Symposium N: Microstructure Processes in Irradiated Materials, Mater. Res. Soc. Proc. 540, Warrendale, PA, 1999, p. 445.
[17] T.R. Allen, J.T. Busby, G.S. Was, E.A. Kenik, J. Nucl. Mater. 255 (1998) 44.
[18] J. Ruzickova, B. Million, Mater. Sci. Eng. 50 (1981) 59.
[19] B. Million, J. Ruzickova, J. Vrestal, Mater. Sci. Eng. 72 (1985) 85.
[20] T.R. Allen, G.S. Was, E.A. Kenik, J. Nucl. Mater. 244 (1997) 278.
[21] J.M. Perks, A.D. Marwick, C.A. English, A computer code to calculate radiation-induced segregation in concentrated ternary alloys AERE R 12121, June, 1986.
[22] A.D. Marwick, R.C. Piller, T.E. Cranshaw, J. Phys F. Met. Phys. 17 (1987) 37.
[23] A. Marucco, Mater. Sci. Eng. A189 (1994) 267.
[24] F. Rotman, D. Gilbon, O. Dimitrov, in: K.C. Russell, D.F. Smith (Eds.), Physical Metallurgy of Controlled Expansion Invar-Type Alloys, The Minerals, Metals, and Materials Society, 1990, p. 145.
[25] C. Dimitrov, D. Huguenin, P. Moser, O. Dimitrov, J. Nucl. Mater. 174 (1990) 22.
[26] M. Nastar, P. Bellon, G. Martin, J. Ruste, T.R. Allen, in: Symposium B: Proceedings of the 1997 MRS Fall Meeting: Symposium B Phase Transformations and Systems Driven Far From Equilibrium, Mater. Res. Soc. Proc. 481, Pittsburgh, PA, 1998, p. 383.